Cryogenics 150 (2025) 104130

Contents lists available at ScienceDirect

Cryogenics

journal homepage: www.elsevier.com/locate/cryogenics

3D effervescence Modeling of a Titan submarine

Jason Hartwig [a,*], Peter Meyerhofer [b], R. Balasubramaniam [b], Ralph Lorenz [c], Anthony Colozza [d], Geoffrey Landis [a], Steve Oleson [a]

[a] NASA Glenn Research Center, Cleveland, OH 44135, the United States of America
[b] Case Western Reserve University, Mechanical and Aerospace Engineering, Cleveland, OH 44106, the United States of America
[c] Johns Hopkins Applied Physics Laboratory, Laurel, MD 20723, the United States of America
[d] HX5, Brookpark, OH 44142, the United States of America

ARTICLE INFO

Keywords:
Titan
Ligeia
Submarine
Effervescence
Nitrogen/methane/ethane
Bubble incipience

ABSTRACT

An extraterrestrial submarine was studied to explore Saturn's moon Titan, under a Phase II NASA Innovative Advanced Concepts (NIAC) study. One of the primary design concerns for the submarine is the effect of effervescence on submarine operation. Nitrogen gas is highly soluble in Titan's methane-rich sea, Ligeia Mare. Waste heat from the submarine power system may cause this dissolved nitrogen gas to come out of solution; in a quiescent case, bubbles that form may interfere with science instruments, and in a moving case, bubbles that form along the submarine may coalesce at the aft end and cause cavitation in the propellers. This paper introduces the Phase II orbiter-supported submarine, updated mission profile, critical subsystems, as well as relevant models needed to quantify effervescence as a function of the location and operation within Ligeia Mare. Phase I and Phase II submersible designs are also compared and contrasted.

1. Introduction

The purpose of this paper is to assess the risk of effervescence on the Phase II submarine design being assessed to explore the cryogenic methane-rich sea Ligeia Mare of Saturn's moon Titan. Effervescence is defined throughout to be the formation of gas bubbles in a liquid by a change in temperature or pressure of the liquid. This vehicle is being designed as part of a NASA Innovative Advanced Concepts (NIAC) Phase II study for a science mission to explore Ligeia Mare for a ~ 1 year mission. The formation, growth, and location of bubbles, and thus effervescence, was identified as a major risk to the proposed science mission.

The outline of this paper is as follows. First, the Titan cryogenic environment is introduced. Next, the new Phase II vehicle and updated mission concept of operation are presented. Then the new 3D effervescence model is described; solubility, bubble incipience, bubble growth, and area and volume coverage models are described. Finally, the results of the effervescence model are presented and assessed, particularly for impact on science instruments and propeller operation.

1.1. Titan environment

Processes on Titan share many similarities with processes on Earth, except they occur at significantly lower temperatures[15,16,18]. The surface temperature on Titan is ~ 93 K and the atmospheric pressure is ~ 1.5 atm with a gravitational acceleration of 1.35 m/s^2. The surface atmosphere composition is approximately 95 % nitrogen and 5 % methane by mole fraction. Furthermore, Titan is the only known place in the Solar System other than Earth that has stable, exposed bodies of surface liquid, i.e. seas. Other icy moons such as Europa and Ganymede are believed to have internal water oceans, which Titan likely also has, but these seas lie beneath tens to hundreds of kilometers of ice and are not considered here. The seas of Titan are concentrated near the north pole, and are composed of liquid methane and liquid ethane in varying proportions. The methane evaporates, forms low-altitude clouds, and returns back to the surface as rain in an analogue to the hydrological cycle on Earth, while ethane is not sufficiently volatile to be present in this process in large quantities. As such, Titan represents a unique and unprecedented design challenge for submersibles capable of exploring the cryogenic seas.

1.2. Phase II submarine and mission

Recently, a 1300 kg, 6.5 x 1.2 x 0.8 m^3 submarine was designed to explore Kraken Mare under a NIAC Phase I study, shown in Fig. 1 [21] and [7]. At the cost of very low data transmission rates, this version was a stand-alone design with capability to perform direct-to-Earth (DTE)

* Corresponding author.

https://doi.org/10.1016/j.cryogenics.2025.104130
Received 5 February 2025; Received in revised form 18 May 2025; Accepted 27 May 2025
Available online 4 June 2025
0011-2275/Published by Elsevier Ltd.

Nomenclature

Units

Area A m^2.
Normalized mass concentration C dimensionless.
Drag coefficient C_D dimensionless
Diffusion coefficient D m^2/s.
Force F Newtons.
Gravitational acceleration g m/s^2.
Height H meters.
Length L meters.
Nucleation site density N_n $1/m^2$.
Number n
Pressure P MegaPascals.
Excess above vapor pressure P^* MegaPascals
Heat transfer $\dot{Q}$ Watts.
Bubble radius R meters.
Reynolds number Re dimensionless.
Supersaturation S dimensionless.
Temperature T Kelvin.
Time t seconds.
Width W meters.
Volume V m^3.
Volume flow rate $\dot{V}$ m^3/s.
Velocity v m/s.
Propeller velocity change Δv m/s.
Coordinate position x, y, z meters.
Mole fraction $x_{()}$ dimensionless.

Greek

Bubble growth constant β dimensionless.
Surface tension γ N/m.
Similarity variable η dimensionless.
Contact angle θ degrees or radians.
Kinematic viscosity ξ m^2/s.
Density ρ kg/m^3.
Density ratio ρ^* dimensionless.
Solidity ratio σ dimensionless
Area or Volume coverage ϕ dimensionless

Subscripts

b	buoyancy force.
c	critical bubble radius.
cr	maximum growth time in quiescent case.
dr	drag force.
front	submarine front (projected).
g	nitrogen vapor in bubble.
l	Titan seas.
nc	induced velocity due to natural convection.
p	low-pressure region behind the propellers.
sub	submarine dimensions or speed.

communication, in the absence of an orbiter to relay signals around Saturn back to Earth. DTE communication also implied that a significant portion of that mission was spent floating at the surface transmitting data. A radioisotope power system provided power and heat for the submarine through the mission, providing heat to keep the electronics at Earth temperatures, a goal aided by a layer or aerogel insulation under the submarine skin. The waste heat is released into the surroundings through the submarine exterior surface. The 370 W/m^2 of waste heat flux could potentially cause dissolved nitrogen gas to come out of solution. Subsequently, a 1D effervescence model was developed to examine the effect of heat flux and pressure drop on the formation, growth, and coverage of bubbles on the submarine [9]. Results showed that the waste heat flux was not high enough to cause significant area or volume fraction of bubbles to hinder the operation of the Phase I submarine, primarily because the ethane-rich Kraken Mare does not hold much nitrogen gas.

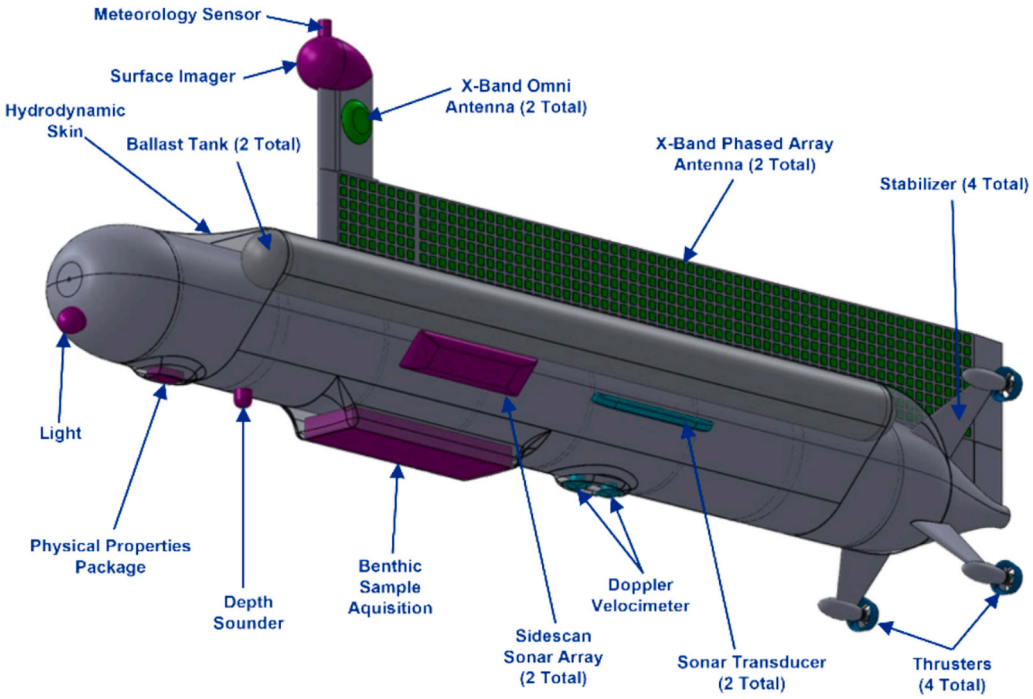

Fig. 1. Phase I Submarine Concept from Oleson et al. (2016).

Meanwhile, the Phase II submarine shown in Fig. 2, similar in shape and design as a sea turtle, is expected to traverse the methane-rich Ligeia Mare, where there is higher nitrogen concentration, and thus higher propensity for effervescence. The design of the new submarine reflects the requirement for sensors that cover liquid, seabed and atmosphere measurements, as well as a similar radioisotope power system and the communication system that sends the data to Earth. As in the Phase I design, other requirements for the turtle include autonomous operation, a total mission life of a year or longer and the structural integrity to withstand 5-g axial loads and 2-g lateral loads at launch. The body shape is approximately an ellipsoid and the vehicle is carried in an axisymmetric aeroshell for entry to the Titan atmosphere. For reference and comparison, Table 1 shows important features of the Phase I and Phase II submersible concepts. Table 2 outlines specific dimensions of the Phase II turtle, along with relevant information needed to make subsequent effervescence calculations.

Fig. 3 outlines the Phase II mission concept of operation. The Phase II design is intended to be packaged with an orbiter, so that the submarine may be lighter and smaller, while still preserving all of the primary science objectives. While the mission cost may rise due to launching both submersible and orbiter, the mission could commence as early as the late-2020 s, depending on availability of required technology. Furthermore, with an orbiter-based mission, the effect of the seasons on positioning the submarine to relay data back to Earth is eliminated.

Table 1
Submarine Design Requirements for Phase I and Phase II.

	Phase I	Phase II
Hydrocarbon composition (targeted sea)	Any methane-ethane proportion (Kraken and Ligeia)	Methane-rich (Ligeia)
Mass (kg)	1386	530
Power (W)	~800	~100
Waste heat (W/m^2)	370	300
Science/measurement mass (kg)	80	80
Size	6.5 m long, 1.2 m wide, 0.8 m high, ~2.77 m^3	2 m long, 1.4 m wide, 0.7 m high, ~1 m^3
Entry, descent and landing	~8 m lifting body	2.7 m aeroshell
Primary mission on Titan	90 days	1 year
Average Speed (m/s)	1	0.1
Range (km)	>4000	>2000
Depth limit (m)	1000	200
Ballast system	Reclaimable cold gaseous helium (GHe) or neon (GNe)	Consumable warm gaseous helium or Bellows
Number of dives (duration)	~90 (8 h submerged, 16 h surfaced)	~25 (12 days submerged, 4 days surfaced)
Data relayed (schedule)	1 Gb (800 bps for 16 h per day)	1 Gb (100 kbps for 30 min every 5 h)

1.3. Problem Statement

The chemistry and the cryogenic temperatures of Titan make the design of this extraterrestrial submarine more challenging than any submersible design on Earth. Fig. 4 shows a block diagram of the Phase II submarine internals, as well as the temperature gradient across the sub. Waste heat is distributed from the power system, and along with the appropriately sized insulation thickness, the science equipment is maintained at ambient conditions. Ultimately, the waste heat is rejected into the surrounding sea. As shown in Fig. 4, there is a significant temperature gradient between the power system and sea. This temperature difference is not likely to cause local boiling of the liquid, but it may be enough to cause nitrogen gas that is dissolved in the liquid to come out of solution.

The difficulty for the current Phase II submarine design is that the solubility of nitrogen in liquid methane is relatively high[20] and [8], which may result in gas coming out of solution if the sea is saturated and the solubility limit decreases due to waste heat leak or pressure drop. For comparison, the mole fraction solubility of air in water is negligible [https://www.engineeringtoolbox.com/air-solubility-water-d_639.html .] [1]. Effervescence raises two main issues:

1. In a quiescent or hovering case, bubbles that form may interfere with instrumentation, e.g. [2]. This would jeopardize critical science mission objectives.
2. In a moving case, bubbles that form may coalesce and cause cavitation in the propellers, potentially hindering control and navigation, causing loss of thrust, or damaging the blades.

The 1D effervescence model was developed in[7]for a slender (i.e. large L/D) submarine from Phase I. Core elements of this model can be

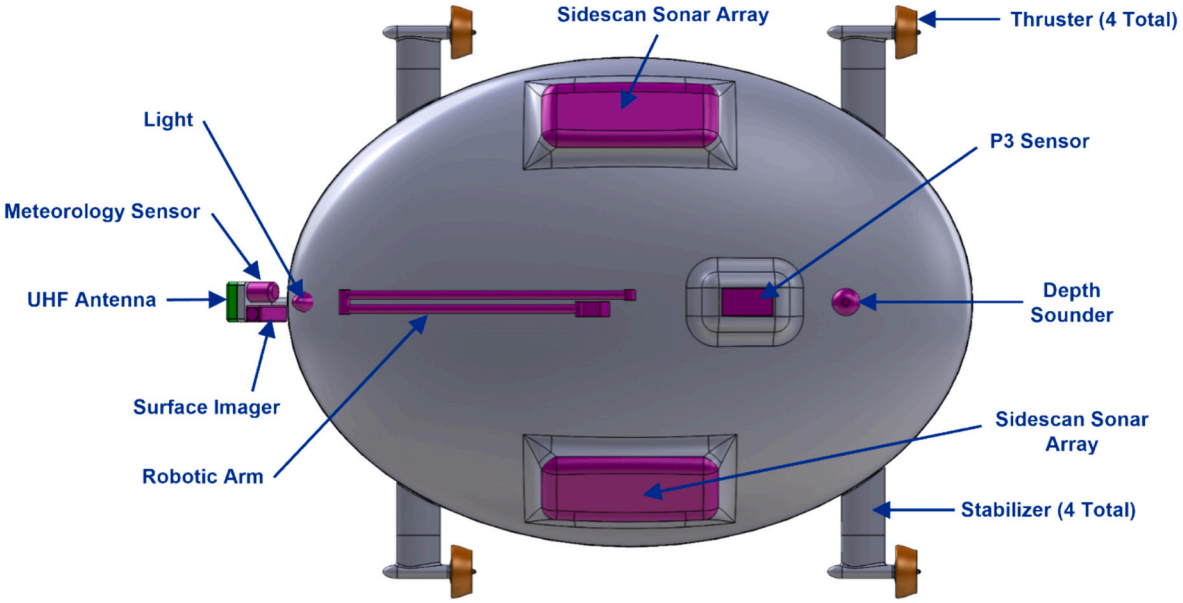

Fig. 2. Phase II Submarine Concept.

Table 2
Phase II Relevant Dimensions and Features Needed to Compute Effervescence.

Quantity	Value
Propeller length L_{prop} [m]	0.117
Propeller width W_{prop} [m]	0.14
Propeller height H_{prop} [m]	0.14
Length L_{sub} [m]	2
Width W_{sub} [m]	1.4
Height of main body (excluding communication array) H_{sub} [m]	0.7
Skin temperature T_{skin} [K]	Variable
Sea temperature T_{bulk} [K]	93
Travel speed v_{sub} [m/s]	Variable
Waste heat $\dot{Q}_{waste}$ [W]	Variable
Titan gravity g [m/s^2]	1.35
Convection coefficient h [W/m^{2}K]	Variable
Diffusion coefficient of nitrogen in liquid methane D [m^2/s]	$2*10^{-9}$ [6]

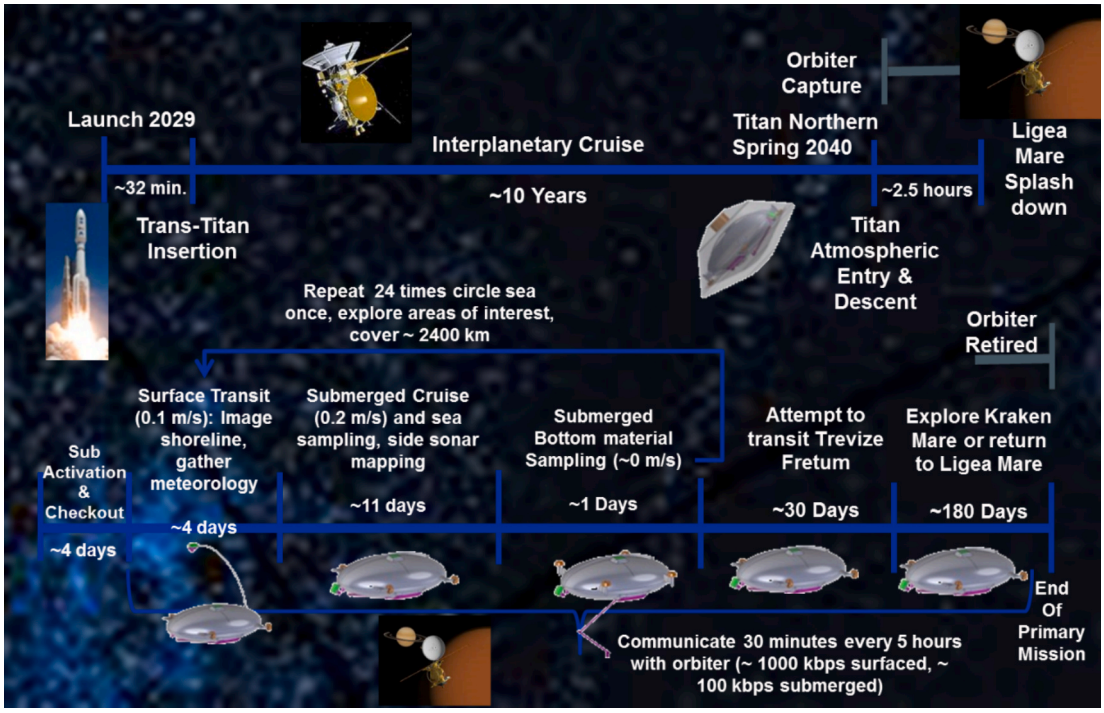

Fig. 3. Phase II Mission Concept of Operation.

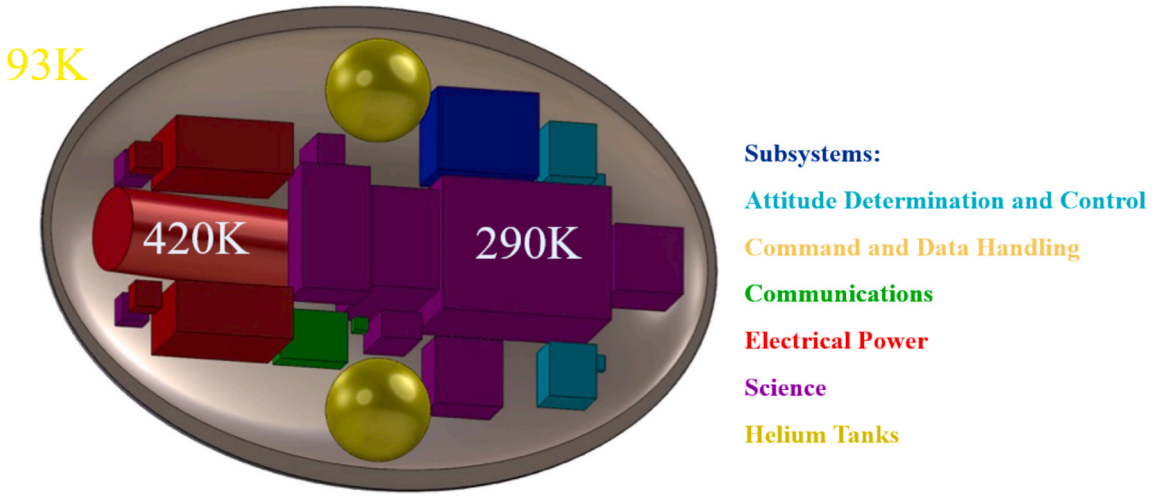

Fig. 4. Heat Flow and Internals of the Phase II Submarine. Blocks are shown for subsystems.

used for the wider Phase II turtle submarine, but bubble area and volume coverage models must be redeveloped based on the new geometry and slower cruising velocity of the new design. Therefore, the goal of this study is to quantify the bubble area and volume coverage to determine if the submarine requires modification in design (ex. rerouting waste heat to the top of the craft).

2. Modeling

2.1. Solubility

The core models of the effervescence model for skin temperature, solubility, bubble incipience, and bubble growth remain unchanged; only a brief description of those is given here, with details presented in [8]. Details of the skin temperature calculations as a function of waste heat are presented in[7]. Supersaturation is defined as the ratio of the difference in the dissolved solute concentration in the liquid and the bubble surface, to that at the bubble surface:

$$S = \frac{x_b - x_i}{x_i} \tag{1}$$

where x is the mole fraction of the solute (dissolved gas) in the liquid, and subscripts b and i denote bulk liquid (at Titan sea temperature) and interface (at submarine skin temperature) values, respectively. The first step is to calculate x_b and x_i. A correlation for ternary ethane/methane/nitrogen mixtures representative of Titan seas was developed in [8], which gives the mole fraction solubility of nitrogen, is:

$$\frac{x_{N2}}{P^*} = a_0 \exp\left(a_1 T + a_2 T^2 + a_3 P^* + a_4 T P^* + a_5 T^2 P^*\right)\left(\frac{x_{C1}}{x_{C1} + x_{C2}}\right)^{a_6} \tag{2}$$

where x_{C1} and x_{C2} are the mole fraction of LCH_4 and LC_2H_6, respectively. The values a_0 to a_6 are coefficients listed in Table 3. The pressure variable P^* is the excess above vapor pressure, in MPa. The vapor pressure used is that of the binary methane-ethane mixture. Eq. (2) can be used to determine the mole fraction solubility of gaseous nitrogen given a ratio of liquid methane to liquid ethane, at any temperature or pressure (depth) of the Titan seas.

2.2. Bubble incipience

Based on general descriptions[25] and [13]of bubble nucleation theory, the only plausible way for the submarine to induce effervescence is at pre-existing gas cavities on the surface; the values of supersaturation are nowhere near large enough for nucleation to occur in open liquid. The same point is reinforced by the highly wetting nature of cryogenic liquids[6]. The active nucleation site density on surfaces in boiling systems is well researched, see for example[26] and Hibiki and Ishi (2003). Very few quantitative studies appear to exist for gas evolution on surfaces in contact with supersaturated solutions[14] and [22]. For analysis in the current work, the model of[11]is employed, modified for effervescence in place of boiling. The model equations are:

Table 3
Fitted Coefficients for Nitrogen Solubility in Methane/Ethane Solvent, 90–100 K.

$\mathbf{a_0}\,(\mathbf{MPa^{-1}})$	46.5
$\mathbf{a_1}\,(\mathbf{K^{-1}})$	−0.0439
$\mathbf{a_2}\,(\mathbf{K^{-2}})$	−0.00001
$\mathbf{a_3}\,(\mathbf{MPa^{-1}})$	3.07
$\mathbf{a_4}\,(\mathbf{MPa^{-1}K^{-1}})$	−0.000044
$\mathbf{a_5}\,(\mathbf{MPa^{-1}K^{-2}})$	−0.00001
$\mathbf{a_6}$	0.933

$$N_n = \overline{N}_n\left(1 - \exp\left(-\frac{\theta^2}{8\mu^2}\right)\right)\left(\exp\left(f(\rho^+)\frac{\lambda}{R_c}\right) - 1\right) \tag{3}$$

$$f(\rho^+) = -0.01064 + 0.48246\rho^+ - 0.22712(\rho^+)^2 + 0.05468(\rho^+)^3 \tag{4}$$

$$\rho^+ = \log(\rho^*) \tag{5}$$

$$\rho^* = \frac{\rho_l - \rho_g}{\rho_g} \tag{6}$$

where R_c is the critical bubble radius for nucleation, $\overline{N}_n = 4.72{*}10^5$ sites/m^2 (used as m^{-2} since counting sites is dimensionless), θ is the liquid–solid contact angle at the liquid–vapor interface (rad), $\mu = 0.722$ rad, $\lambda = 2.5{*}10^{-6}$ m, ρ_l is the saturated liquid density of the pure solvent (the methane-ethane mixture) and ρ_g is the saturated vapor density of the pure solute (nitrogen). Equations (3) to (6) are used together with an expression for critical radius to compute nucleation site density, in nucleations per m^2. The adaptation from boiling to effervescence concerns the critical radius:

$$R_c = \frac{2\gamma}{P_a S} \tag{7}$$

where γ is the surface tension of the pure solvent, P_a is the ambient pressure (written in Pa, not MPa, to resolve units to meters), and S is the supersaturation from Eq. (1).

2.3. Bubble growth

Scriven [(1959) developed a model for the spherically symmetric growth of a single-component bubble in a liquid of infinite extent driven by both heat and mass transfer; for a single component gas, growth is driven by diffusion of gas in the liquid around the bubble. Multicomponent gas bubbles were addressed in[4]. It is assumed that bubbles do not interact with the submarine surface or with each other (i.e. they do not combine), such that spherical symmetry holds.

Scriven [24] defines the bubble radius as:

$$R(t) = 2\beta\sqrt{Dt} \tag{8}$$

where β is a growth constant evaluated numerically from:

$$2\beta^2 \int_0^1 \exp\left[-\beta^2\left(\frac{1}{(1-x)^2} - 2\left(\frac{\rho^*}{1+\rho^*}\right)x - 1\right)\right]dx = \frac{(1+\rho^*)x_i S}{1 - \frac{\rho_l}{\rho_g}\left(1 - \frac{\rho^*}{1+\rho^*}\right)} = \frac{(1+\rho^*)x_i S}{1 - \frac{\rho_l}{\rho_l}} \tag{9}$$

for given values of ρ_b, ρ_i, and ρ_g, or equivalently for given values of ρ^*, x_i, and S.

2.4. Bubble volume and area coverage Modeling

Now, new models are needed for how the bubbles accumulate and move along the Phase II submarine to determine both the volume gas fraction in the sea and also bubble area coverage along the submarine. General assumptions are as follows:

- Nucleation sites are uniformly concentrated according to Equations (3) and (4).
- The incipience of bubbles at each site is a continuous stream.
- The growth of each bubble is spherically symmetric and not influenced by the nucleating surface, or by other bubbles, in line with Scriven's assumptions. Bubble growth is therefore given by Equation (8) in the moving and quiescent cases.

- The bubble area used in area coverage calculations is the frontal area of a sphere facing a flat surface (the submarine), a circle of the bubble radius. In other words, each bubble projects an area of πR_{bubble}^2 on the bottom face of the submarine. This is conservative, since some bubbles will block the full projection of other bubbles onto the submarine surface.
- Only bubbles that form on the bottom side are considered in calculations.
- Boundary layer effects are negligible.

In general, the bottom of the submarine has an ellipsoid shape with the same vehicle dimensions in Table 2. The exception to this is the height, which differs between top half (0.3 m) and bottom half (0.4 m), so for the equations in this section, $H_{sub} = 0.7$ meters. The equation of the ellipsoid is

$$\frac{x^2}{(W_{sub}/2)^2}+\frac{y^2}{(H_{sub}/2)^2}+\frac{z^2}{(L_{sub}/2)^2}=1 \tag{10}$$

where x, y, z are the coordinates illustrated in Fig. 5. The derivatives $\frac{\partial y}{\partial x}$, $\frac{\partial y}{\partial z}$ can be computed at any point (x, z) on the bottom surface.

The projected area of the bottom of the submarine is divided into a rectangular grid along the x and z axes. This grid is considered over the ellipse that results from projecting the length and width of the submarine. Let dx be the x-increment of a grid space and dz the z-increment. Bubble nucleation occurs over a surface area which is greater than the projected area, due to the slope of each square $dxdz$; (3D effects are thus accounted for at each point along the 2D grid). This is done as a conservative approach. Applying trigonometry to the surface gives:

$$n_{bub} = N_n dx dz^* \frac{1}{2}\left(\sqrt{1+\left(\frac{\partial y}{\partial x}\right)^2}+\sqrt{1+\left(\frac{\partial y}{\partial z}\right)^2}\right) \tag{11}$$

The accelerations of the bubbles in the x and z directions are considered independently. Each follows from the solution to bubble motion in the absence of a net fluid velocity, which is superimposed; the equations are from[9], and the value of g will be corrected for slope at the end. The buoyancy force on a spherical bubble of radius $R(t)$ is:

$$F_b = g(\rho_l-\rho_g)\frac{4\pi}{3}R(t)^3 \tag{12}$$

and the drag on the bubble, using the appropriate drag coefficient[5], is

$$F_{dr} = 12\pi\mu R(t)\left(\frac{dy}{dt}-v_{nc}\right) \tag{13}$$

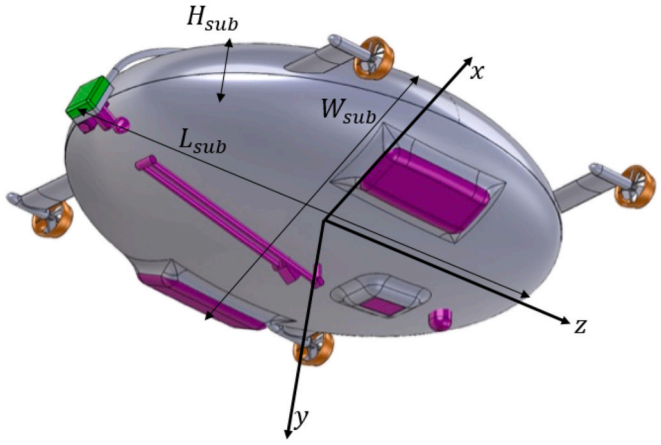

Fig. 5. The Coordinates in the Analysis Superimposed on the Submarine as Viewed from the Bottom. The origin corresponds to the center of the vehicle midplane.

The bubble equation of motion is expressed by Newton's second law:

$$F_b - F_{dr} + F_1 = \frac{4\pi}{3}R(t)^3\rho_g\frac{d^2y}{dt^2} \tag{14}$$

where F_1 is the "added mass" force [3]and v_{nc} is the (assumed constant) speed of natural convection. Setting $v_{nc} = 0$ and solving Equation (14), with initial conditions $y(0) = \frac{dy}{dt}(0) = 0$, gives

$$y(t) = \frac{2(\rho_l-\rho_g)\beta^2 D}{9\mu+(5\rho_l+4\rho_g)\beta^2 D}gt^2 \tag{15}$$

Finally, if the angle of the submarine bottom (above horizontal) is $\theta = \arctan\left(\frac{\partial y}{\partial x}\right)$ (equivalently for z), then g becomes $g\sin(\theta)$ and the bubble acceleration is

$$\frac{4(\rho_l-\rho_g)\beta^2 D}{9\mu+(5\rho_l+4\rho_g)\beta^2 D}g\frac{\left|\frac{\partial y}{\partial x}\right|}{\sqrt{1+\left(\frac{\partial y}{\partial x}\right)^2}}OR-\frac{4(\rho_l-\rho_g)\beta^2 D}{9\mu+(5\rho_l+4\rho_g)\beta^2 D}g\frac{\frac{\partial y}{\partial z}}{\sqrt{1+\left(\frac{\partial y}{\partial z}\right)^2}} \tag{16}$$

The difference in how the signs are treated reflects the flow pattern in the moving case: bubbles always accelerate in the positive x direction but can decelerate in z while they travel down the front surface of the submarine. This result assumes a constant impulse on each grid space.

If a bubble enters a grid space at radius $R_0 = 2\beta\sqrt{Dt_0}$ and the time t_{cross} to leave the space is known, then Equation (8) gives a means of estimating the bubble radius R_1 when the bubble leaves the space. The change in bubble radius is based on a finite difference:

$$R_1 = R_0 + \left.\frac{dR}{dt}\right|_{t_0} t_{cross} = R_0\left(1+\frac{t_{cross}}{2t_0}\right) = R_0\left(1+\frac{2\beta^2 D}{R_0^2}t_{cross}\right) \tag{17}$$

The value of t_{cross} is estimated on each grid space from the dimensions of the space and the speed with which bubbles come onto the space.

Most grid spaces (x_0, z_0) have a flow of bubbles from the spaces $(x_0 - dx, z_0)$ (subscript left) and $(x_0, z_0 - dz)$ (subscript rear) in addition to the bubbles nucleated at that space. Because tracking the branching bubbles from each square would be unduly expensive to compute, the 3 flows are combined into one. This combination conserves volume, number of bubbles, and momentum to estimate the average bubble speed and radius. The new radius is

$$\overline{R} = \sqrt[3]{\frac{n_{new}R_{new}^3 + n_{left}R_{left}^3 + n_{rear}R_{rear}^3}{n_{new}+n_{left}+n_{rear}}} \tag{18}$$

and the new bubble velocity is:

$$\overline{v} = \frac{n_{new}R_{new}^3 v_{new} + n_{left}R_{left}^3 v_{left} + n_{rear}R_{rear}^3 v_{rear}}{(n_{new}+n_{left}+n_{rear})\overline{R}^3} \tag{19}$$

This velocity simplification is applied in the x and z directions separately.

The proportion of bubbles that travel forward into the square $(x_0, z_0 + dz)$ and the proportion that travel right into $(x_0 + dx, z_0)$ depend on average, on the velocities $\overline{v}_x$, $\overline{v}_z$. If the net velocity is at the same angle to the z axis (in the xz plane) as the diagonal of the grid space, then the aggregate bubbles split half and half between traveling to $(x_0, z_0 + dz)$ and to $(x_0 + dx, z_0)$. In general, this is expressed as:

$$n_{left}|(x_0+dx, z_0) = (n_{new}+n_{left}+n_{rear})\frac{\frac{\overline{v}_x}{\overline{v}_z}}{\frac{dx}{dz}+\frac{\overline{v}_x}{\overline{v}_z}} \tag{20a}$$

$$n_{rear}|(x_0, z_0 + dz) = (n_{new} + n_{left} + n_{rear}) \frac{\frac{dx}{dz}}{\frac{dx}{dz} + \frac{\bar{v}_x}{\bar{v}_z}} \tag{20b}$$

In this way, bubbles propagate from the rearmost, leftmost grid space (with the smallest value of both x and z) to all other spaces.

The area coverage at each grid space is given as the sum of projected bubble areas over a surface area:

$$\varphi_{area} = \frac{(n_{new} + n_{left} + n_{rear})\pi \bar{R}^2}{\frac{1}{2} W_{sub} dz} \tag{21}$$

The reported area fraction is the 95th percentile of area fraction over the whole grid (to exclude outliers). The final expressed solution for volume coverage is the expression:

$$\varphi_{vol} = \frac{(n_{new} + n_{left} + n_{rear})\frac{4\pi}{3}\bar{R}^3}{\frac{\pi}{4} H_{prop}^2 dz} \tag{22}$$

evaluated at the rear propeller position (90 % of the submarine length from the nose). The denominators in Eq. (21) and (22) are chosen to ensure grid independence.

2.4.1. Moving case

Fig. 6 shows the grid and path of the bubbles in the moving case. Only half the bottom area of the submarine is used in this case, as divided lengthwise down the middle, because the other half is the same due to symmetry. The domain covered is:

$$|z| < \frac{L_{sub}}{2},\ 0 < x < W_{sub}\sqrt{\frac{1}{4} - \left(\frac{z}{L_{sub}}\right)^2} \tag{23}$$

Grid convergence in Ligeia Mare was conducted at a cruising speed of 0.2 m/s. The contours and the magnitude of ϕ_{vol} are consistent. The magnitude is the most important factor on the submarine, while the shaping is intended only for heuristic purposes. Therefore, the chosen grid size is 400x400 cells on each quarter of the submarine bottom.

2.4.2. Quiescent case

Fig. 7 shows the grid and path of the bubbles in the quiescent case. Here, the analysis covers a quarter of the bottom area of the submarine, because each quarter behaves identically. The domain covered is:

$$0 < z < \frac{L_{sub}}{2}, 0 < x < W_{sub}\sqrt{\frac{1}{4} - \left(\frac{z}{L_{sub}}\right)^2} \tag{24}$$

The natural convection speed at each grid space on the surface is

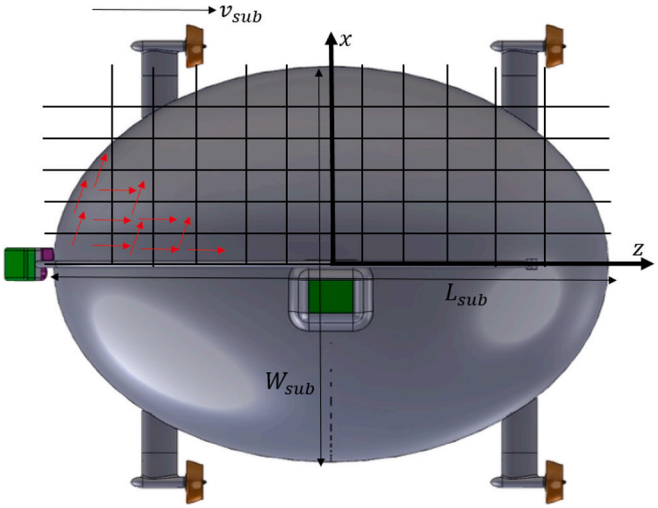

Fig. 6. Path Followed by Average Bubbles in the Moving Case.

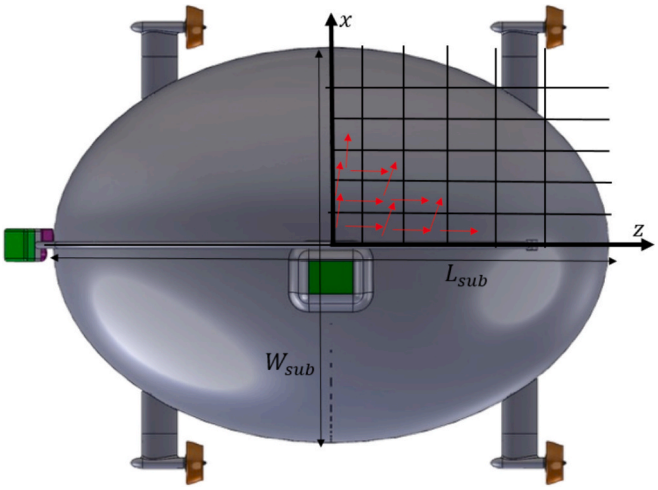

Fig. 7. Path Followed by Average Bubbles in the Quiescent Case.

estimated by a locally flat approximation. The speed of the flow up the submarine side due to natural convection is based on a laminar similarity solution for a vertical flat plate[12]:

$$v_{nc,\max} = \frac{2\xi f \mathrm{Gr}_{x_c}^{1/2}}{x_c} = 2f\sqrt{g\beta_l(T_{skin} - T_b)x_c} \tag{25}$$

where x_c is a variable distance. By numerical approximation, the peak values of f based on a function arising in the solution of differential equations depend on Prandtl number: $f = 0.2119Pr^{-0.302}$ ($Pr > 0.5$). For the grid spaces with the lowest value of x, the $x-$component of the natural convection velocity (where g is changed by according to the local $x-$slope) is given by:

$$u = 2f\sqrt{\beta_l(T_{skin} - T_b)dx^* g \frac{\left|\frac{\partial y}{\partial x}\right|}{\sqrt{1 + \left(\frac{\partial y}{\partial x}\right)^2}}} \tag{26}$$

For other grid spaces, where the flow enters with a non-zero velocity u_0, that speed corresponds to an equivalent distance:

$$x_0 = \frac{u_0^2}{4f^2\beta_l(T_{skin} - T_b)g} \frac{\sqrt{1 + \left(\frac{\partial y}{\partial x}\right)^2}}{\left|\frac{\partial y}{\partial x}\right|} \tag{27}$$

The velocity of the fluid when it leaves the square is then roughly a finite difference:

$$u_1 = u_0 + \left.\frac{du}{dx}\right|_{x_0} dx = u_0\left(1 + \frac{2f^2\beta_l(T_{skin} - T_b)}{u_0^2} g \frac{\left|\frac{\partial y}{\partial x}\right|}{\sqrt{1 + \left(\frac{\partial y}{\partial x}\right)^2}} dx\right) \tag{28}$$

Although not shown for brevity, a similar grid convergence study was done as in the moving case. Again, the chosen grid is 400x400 cells for the quiescent case.

2.5. Pressure drop in propellers

The last major component of effervescence on the submarine is that due to the pressure drop through the propellers. This mechanism is taken from[9]. The model used for the pressure drop of the flow into the propellers is the Bernoulli relation, constrained by the thrust required to

match the submarine drag coefficient$C_D = 0.2$:

$$P - P_1 = \frac{1}{2}\rho_l v_{sub}^2 \left[\left(-1 + \sqrt{1 + C_D \frac{A_{front}}{4A_p}} \right) + \frac{1}{4}\left(-1 + \sqrt{1 + C_D \frac{A_{front}}{4A_p}} \right)^2 \right] \quad (29)$$

where $A_{front} = 0.77\ \mathrm{m}^2$ is the submarine frontal area and $A_p = \frac{\pi}{4}H_{prop}^2$ is the propeller area. The number of bubbles nucleated at the propeller low pressure depends on the difference between nucleation site densities $N_{n,p}$, N_n calculated from Eq. (3):

$$n_{prop} = \sigma \frac{\pi}{4} H_{prop}^2 (N_{n,p} - N_n) \quad (30)$$

where σ is the solidity of the propellers (the ratio of the blade surface area to the projected area of the duct) and is set at 0.5 based on pictures of the submarine. The volume of a line of bubbles from a single nucleation site is shown in Fig. 8 and given by:

$$V_{line} = \int_0^{0.5L_{prop}} \pi (R(t_x))^2 dx = \int_0^{0.5L_{prop}} \pi \left(R\left(\frac{x}{v_{sub}} \right) \right)^2 dx = \frac{\pi \beta^2 D L_{prop}^2}{2 v_{sub}} \quad (31)$$

Finally, the reference volume, to which the bubble stream is compared, is the disk filling the aft half of the propeller casing: $0.5L_{prop}\frac{\pi}{4}H_{prop}^2$. Adding the two volume fractions in the moving case, the result is:

$$\varphi_{vol,p} = \varphi_{vol}|_{at\ blade} + \frac{n_{prop} V_{line}}{0.5 L_{prop} \frac{\pi}{4} H_{prop}^2} = \varphi_{vol}|_{at\ blade} + \frac{\pi \alpha (N_{np} - N_n) D \beta^2 L_{prop}}{v_{sub}} \quad (32)$$

The quiescent case is not analyzed here because the startup entrained flow speed through a propeller is substantially more complicated.

2.6. Method of solution

The method of solution is as follows:
Thermally driven effervescence.

1. Choose whether the submarine is quiescent or moving. This specifies the Nusselt number correlation to use for skin temperature from[7]or [9]. For the moving case, also specify the submarine velocity.
2. Choose a location within Ligeia Mare. This determines P, T_{bulk}, x_{CH4}, and x_{C2H6}; these four variables uniquely specify ρ^* and D.
3. Use relations from[7]or[9]to compute the submarine skin temperature as a function of waste heat flux.
4. Use Equation (2), with the coefficients in Table 3, to determine x_i and x_b, and thus S from Equation (1).
5. Determine the critical radius from Equation (7), then use Equation (3) to determine the number of nucleation sites per square meter.
6. Solve Equation (9) for the bubble growth constant β.
7. Finally estimate bubble area and volume fractions due to thermal effects from the discussion around Equations (21) and (22).

Pressure driven effervescence.
In the moving case, use Equation (32).

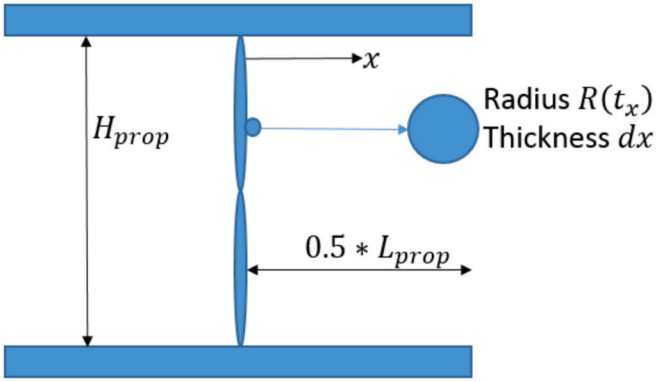

Fig. 8. An Illustration of How Bubbles Grow in the Propeller Cavity.

3. Numerical results and discussion

All subsequent simulations were run for a solvent composition of 85 parts methane to 15 parts ethane, which when using the solubility model, corresponds to 74/13/13 methane/ethane/nitrogen mole fractions, corresponding to Ligeia Mare[10]for the quiescent case and at a speed of 0.2 m/s for the moving case. The diffusion coefficient value D used in the calculations is quoted in Table 2. The present design of the submarine has a waste heat flux of 300 W/m^2. At this value, the skin temperature is expected to be less than 96 K, as shown in Fig. 9. The skin is warmer in the quiescent mode, because forced convection provides better heat transfer than natural convection.

The solubility limit in Equation (2) is shown graphically in Fig. 10 for Ligeia Mare. The maximum pressure of 0.3 MPa is based on the density of the sea and the estimated depth of 200 m[19]. The trends are that solubility rises with increasing pressure, decreasing temperature, and increasing methane mole fraction[8]. If the bulk liquid is already saturated, heating the submarine surface will reduce solubility and cause supersaturation.

Table 4 presents results of the parametric simulations at various vehicle velocities, contact angles, and sea temperature and pressure where φ_{area}, φ_{vol}, and $\varphi_{vol,p}$ are the area coverage and volume coverage before and after propellers, respectively. For all cases, the waste heat flux is 300 W/m^2 and methane fraction is 0.85. Varying pressure simulates the effect of depth, and the equilibrium solubility is taken at the high pressure value (where it is higher). Compared to results from Hartwig et al. [7], results here show that effervescence is a much greater problem in methane-rich seas than it is in ethane-rich seas. This is attributed to the fact that methane rich seas have a higher supersaturation than ethane rich seas. In turn, this amplifies both the number of nucleation sites and the bubble growth rate.

The highest area coverage for the cases in Table 4 is 3 %, and the highest volume fraction is 0.0254 %. These extremes occur in the quiescent, high pressure, $\theta = 15$ degree case. For other cases, especially

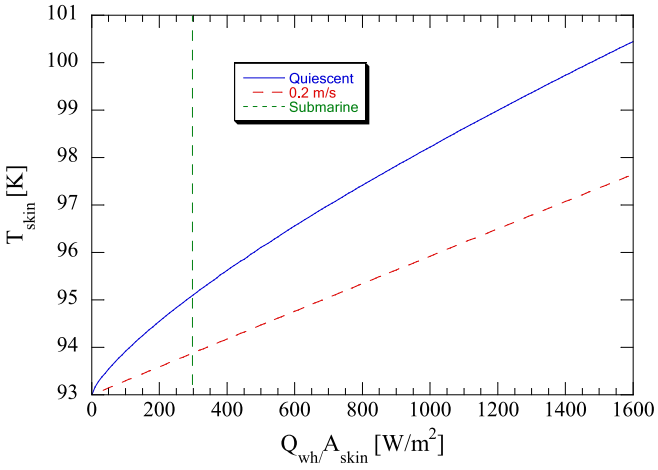

Fig. 9. Submarine Skin Temperature as a Function of Waste Heat Flux, with Sea Temperature 93 K and Given Geometry.

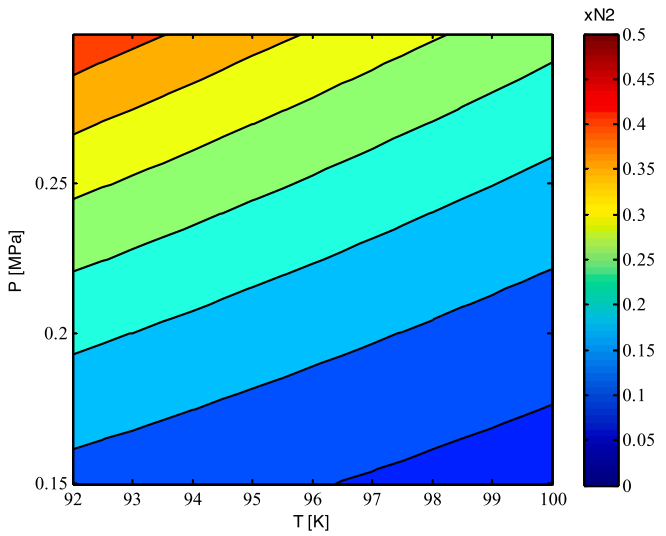

Fig. 10. Equilibrium Solubility of Nitrogen in Methane and Ethane for a Methane-Rich Sea.

where $\theta = 1$ degree, area and volume coverages are orders of magnitude smaller. Figs. 11 and 12 plot the maximum volume fraction and area coverage value, respectively, for this worst case, as a function of sea temperature and pressure. It is clear that more bubbles accumulate in the quiescent cases than in the moving cases, due to the submarine having a shallow bottom that prevents bubbles from quickly dispersing by natural convection alone. Higher area and volume coverage occur at colder liquid temperatures and higher pressures at depth.

The area coverage in this worst case is visualized in Fig. 13. Every point on the curved surface of the submarine, approximated as an ellipsoid, is described as y(x, z). The slope in each Cartesian direction is dy/dx, dy/dz; because L_{sub} is larger than W_{sub}, the relationship between them is dy/dx > dy/dz. This causes a stream of bubbles to be pulled, under the influence of buoyancy, more in the x direction than in the z direction. Bubble area and volume accumulation are therefore biased toward the side of the submarine, instead of the front, along the streamlines of bubble flows. These features could only be captured using a 3D effervescence model; if one used a 2D model where the submarine underside was a flat plane, then the above argument would not hold, and due to a longer path length in z relative to x, more bubbles would accumulate and migrate in the z-direction instead.

The gas volume fraction after the propellers is determined using baseline propeller parameters. The results of this assumption are shown in Fig. 14 for case 6. Compared to Fig. 11, the difference is very small and thus unlikely to affect submarine performance.

Compared to results from[9], The Phase I submarine at 370 W/m^2 waste heat yields a relatively higher skin surface temperature, and correspondingly higher amount of gas coming out of solution, and higher propensity to nucleate and grow bubbles. In the moving case, the Phase I vehicle travels at a higher velocity, and thus there is higher volume coverage before and after the propellers, due to a higher pressure drop. For equal sea mole fraction, temperature, and pressure in both moving and quiescent cases, the total bubble area and volume coverages are higher for the higher waste heat flux submarine from Phase 1 compared to the new Phase II version. For example, for case 6 with the Phase I submarine, the area and volume coverages are 5.5 % and 0.076 %.

Finally, this model can be compared to recent heat flux data using mixtures representative of Titan seas and temperatures[23] as shown in Fig. 15. The data shows the required heat flux needed for bubble incipience as a function of nitrogen mole fraction. The submarine operates near 300 W/m^2, which is an order of magnitude or two less than the data. This suggests a safety factor of at least 5 for the present design. The threshold for perturbations in the Titan environment is about 90 W/m^2, as observed on Huygens[17]. However, boiling liquid methane requires very large surface heat fluxes near 50,000 W/m^2.

Table 4
Results of the Parametric Effervescence Model for Several Cases of Interest to the Titan Submarine.

Case	v_{sub} (m/s)	P(MPa)	θ(deg)	T_{skin}(K)	N_n(1/m^2)	Max φ_{area}	Max φ_{vol}	Max $\varphi_{vol,p}$
1	0	0.15	1	95.107	26.493	3.44E-05	2.02E-07	NaN
2	0	0.3	1	95.104	61.783	1.46E-04	1.13E-06	NaN
3	0.2	0.15	1	93.885	8.613	8.50E-07	6.24E-09	6.25E-09
4	0.2	0.3	1	93.828	15.941	2.98E-06	3.28E-08	3.29E-08
5	0	0.15	15	95.107	5912.4	0.0077	4.52E-05	NaN
6	0	0.3	15	95.104	1.38E04	0.0327	2.54E-04	NaN
7	0.2	0.15	15	93.884	1922.1	1.89E-04	1.39E-06	1.40E-06
8	0.2	0.3	15	93.828	3557.5	6.67E-04	7.32E-06	7.34E-06

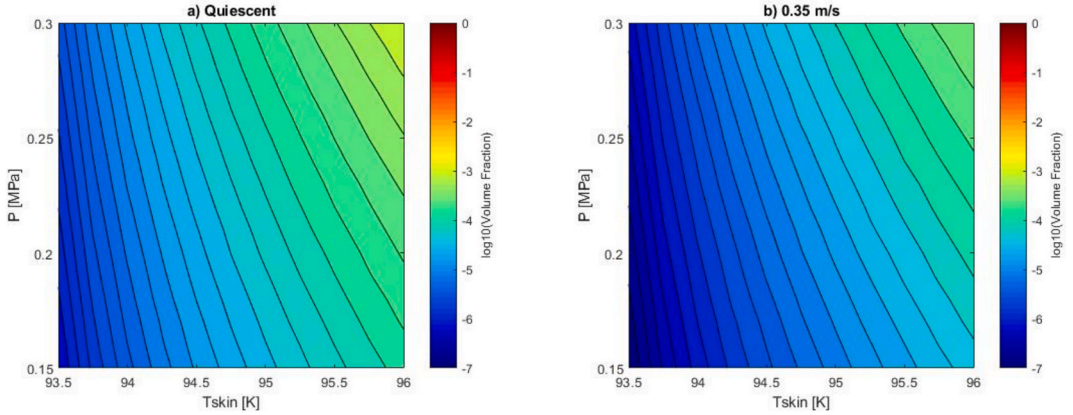

Fig. 11. Log Scale Volume Fraction of Bubbles Around the Propellers for a) Quiescent Case and b) Moving Case. Color bar is set to a maximum of 1.

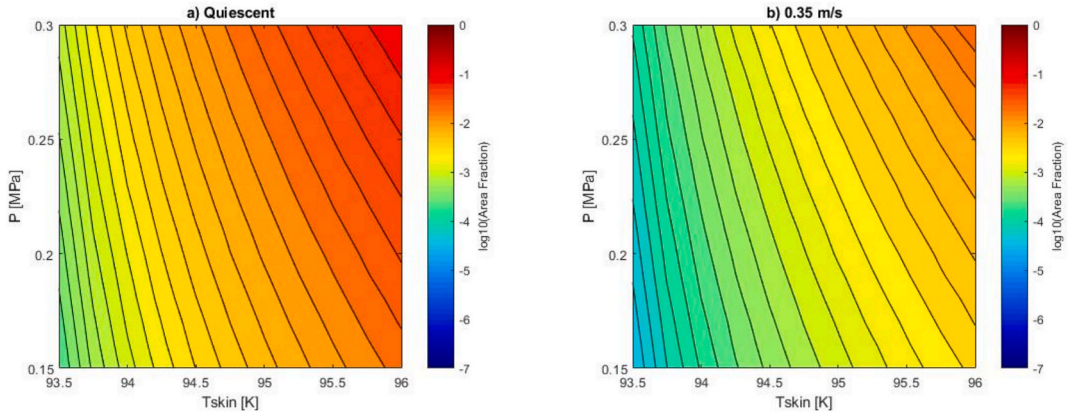

Fig. 12. Log Scale of Area Fraction of Bubbles on the Submarine Skin for a) Quiescent Case and b) Moving Case.

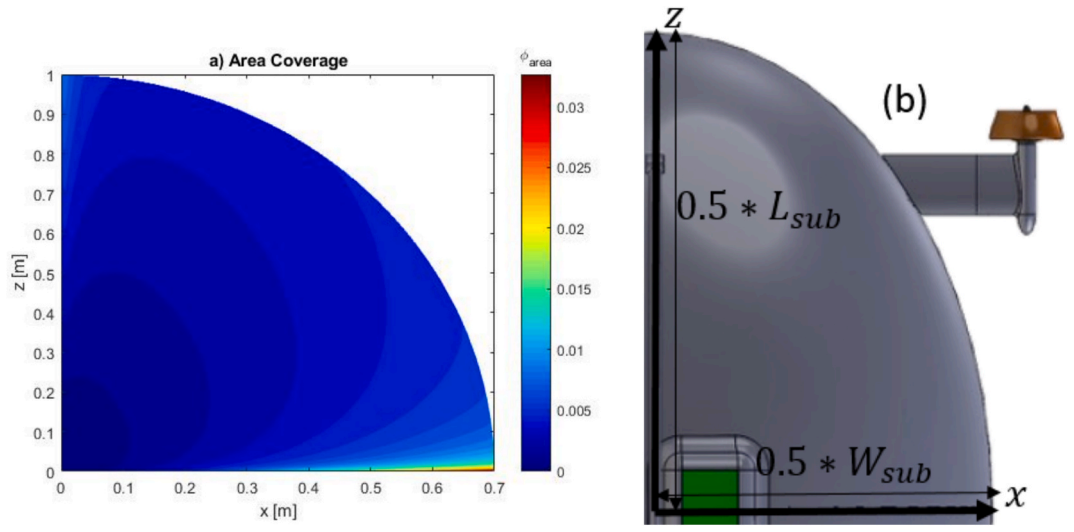

Fig. 13. (a) Visualization of the Area Coverage for the Worst Case in Table 4, Compared to (b) the Submarine.

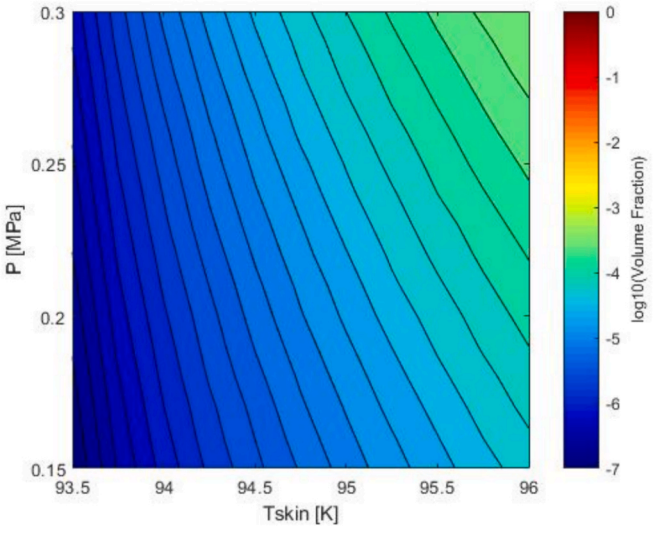

Fig. 14. Volume Fraction after the Propellers, Moving at 0.2 m/s.

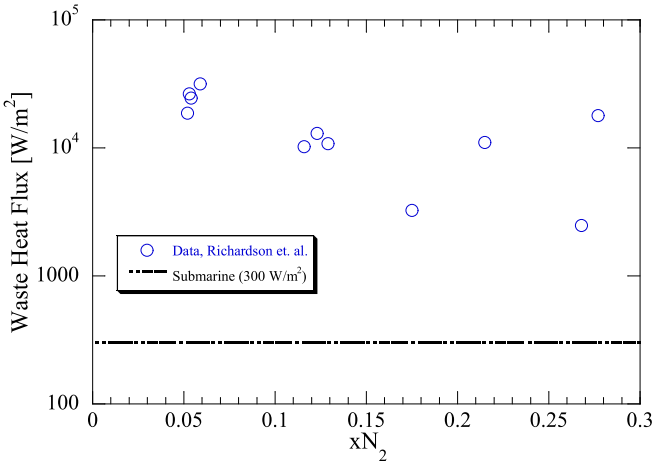

Fig. 15. Comparison of Phase II Operating Point to Experimental Heat Flux Values for Bubble Incipience from Richardson et al. [25].

4. Conclusion

This paper presented a 3D effervescence model by which the incipience, growth, and coverage of bubbles around a submersible body may be approximated in the Titan Ligeia sea. It uses a nucleation site model adapted from boiling studies for effervescence bubbles. When the submarine is in motion, bubbles are swept down the bottom surface while also moving out toward the side by buoyancy. When the submarine is

stationary, bubbles rise up under their own buoyancy, as well as being carried upward in the natural convection induced by vehicle waste heat. The results show that, depending on heat flux, the Titan sea composition and pressure, bubble fractions may occupy reasonably substantial area and volume fractions.

These bubble effects are large enough to potentially impact submarine design. In particular, the skin temperature of any vehicle should be kept less than 97 K, which requires a skin heat flux below 650 W/m^2. Even so, local heat spots might still cause difficulty. In that case, excess heat may be released at a point in the skin of the top surface, away from propellers and instruments. Based on models here, the impact of pressure drop in the propellers on effervescence was shown to be very small at the current operating conditions.

CRediT authorship contribution statement

Jason Hartwig: Writing – original draft, Validation, Software, Methodology, Investigation, Formal analysis, Conceptualization. **Peter Meyerhofer:** Writing – review & editing, Methodology, Formal analysis. **R. Balasubramaniam:** Writing – review & editing, Investigation, Formal analysis. **Ralph Lorenz:** Writing – review & editing, Investigation, Formal analysis, Conceptualization. **Anthony Colozza:** Writing – review & editing, Formal analysis, Conceptualization. **Geoffrey Landis:** Writing – review & editing, Methodology, Investigation, Conceptualization. **Steve Oleson:** Writing – review & editing, Resources, Project administration, Investigation, Funding acquisition, Conceptualization.

Declaration of competing interest

The authors declare that they have no known competing financial interests or personal relationships that could have appeared to influence the work reported in this paper.

Data availability

No data was used for the research described in the article.

References

[1] "Air Solubility in Water," [Online]. Available: http://www.engineeringtoolbox.com/air-solubility-water-d_639.html. [Accessed 13 September 2016].
[2] Arvelo J, Lorenz R. Plumbing the depths of ligeia: considerations for depth sounding in titan's Hydrocarbon seas. J Acoust Soc Am 2013;134:4335–50.
[3] Brennan CE. Fundamentals of multiphase flows. Cambridge University Press; 2005.
[4] Cable M, Frade JR. Diffusion-controlled growth of multi-component gas bubbles. J Mater Sci 1987;22:919–24.
[5] Harper JF. The motion of bubbles and drops through liquids. Adv Appl Mech 1972;12:59–129.
[6] Hartwig JW, Mann JA. Liquid transport in microgravity II: bubble point pressures of Binary methanol/water in fine-mesh screens. Am Inst Chem Eng J 2014;60:730–9.
[7] Hartwig JW, Colozza A, Lorenz R, Oleson S, Landis G, Schmitz P, et al. Exploring the depths of kraken Mare – power, thermal analysis, and ballast control for the saturn titan Submarine. Cryogenics 2016;74:31–46.
[8] Hartwig J, Meyerhofer P, Lemmon E, Lorenz R. An analytical solubility model for nitrogen/ethane/methane Ternary mixtures. Icarus 2017;299:179–86.
[9] Hartwig JW, Meyerhofer P, Balasubramaniam R, Lorenz R, Walsh J, Oleson S. 1D effervescence modeling of an extraterrestrial Submarine in the saturn titan seas. Planet Space Sci 2019;170:1–15.
[10] Hayes AG. The lakes and seas of titan. Annu Rev Earth Planet Sci 2016;44:57–83.
[11] Hibiki T, Ishii M. Active nucleation site density in boiling systems. Int J Heat Mass Transf 2003;46:2587–601.
[12] Incropera FP, DeWitt DP. Fundamental of heat and mass transfer. 5th ed. New York: John Wiley and Sons; 2002.
[13] Jones SF, Evans GM, Galvin KP. Bubble nucleation from gas cavities - a review. Adv Colloid Interface Sci 1999;80:27–50.
[14] Liger-Belair G, Marchal R, Robillard B, Vignes-Adler M, Maujean A, Jeandet P. Study of effervescence in a glass of champagne: frequencies of bubble formation, growth rates, and velocities of rising bubbles. Am J Enol Vitic January 1999;50:317–23.
[15] Lorenz R, Mitton L. in titan unveiled: saturn's mysterious moon explored. NJ, Princeton University Press: Princeton; 2010. p. 180–250.
[16] Lorenz R. "Oceanography on saturn's moon, titan," in MTS/IEEE oceans '13. CA: San Diego; 2013.
[17] Lorenz R. Heat rejection in the titan Surface environment: potential impact on science investigations. J Thermophys Heat Transfer 2016;30:257–65.
[18] Lorenz, R. "The Challenging Depths of Titan's Seas", Journal of Geophysical Research – Planets, 126, 10.1029/2020JE006786. 2021.
[19] Mastrogiuseppe M, Poggiali V, Hayes A, et al. The bathymetry of a Titan Sea. Geophys Res Lett 2014;41(5):1432–7.
[20] Mesli F, Mahboub R, Mahboub M. Molecular dynamics Comparative study of methane-nitrogen and methane-nitrogen-ethane systems. Arab J Chem 2011;4:211–22.
[21] Oleson S, et al. "COMPASS final report. Titan Submarine," NASA CD-2014-114 2014.
[22] Qi Y, Klausner JG. Comparison of nucleation site density for Pool boiling and gas nucleation. J Heat Transfer 2006;128:13–20.
[23] Richardson IA, Hartwig JW, Leachman JW. Experimental effervescence measurements of nitrogen in liquid methane-ethane mixtures. Int J Therm Sci 2019;137:534–8.
[24] Scriven LE. On the dynamics of phase growth. Chem Eng Sci 1959;10:1–18.
[25] Wilt PM. Nucleation rates and bubble stability in water-Carbon dioxide solutions. J Colloid Interface Sci 1986;112:530–8.
[26] Yang SR, Kim RH. A mathematical model of the Pool boiling nucleation site density in terms of the Surface Characteristics. Int J Heat Mass Transf 1988;31:1127–35.